iScience

CellPress
OPEN ACCESS

Article

Dynamic Malignant Wave of Ribosome-Insulted Gut Niche via the Wnt-CTGF/CCN2 Circuit

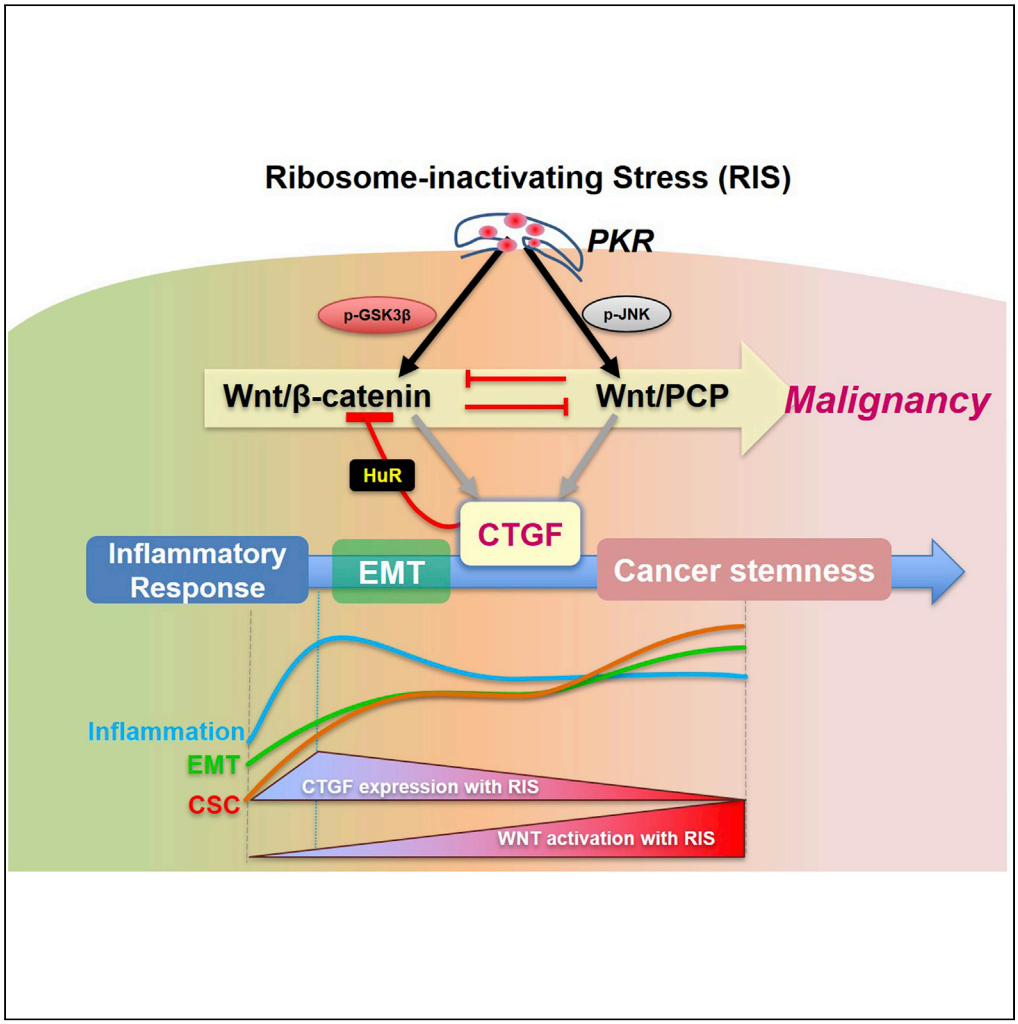

Ki Hyung Kim, Seung Joon Lee, Juil Kim, Yuseok Moon

moon@pnu.edu

HIGHLIGHTS

PKR expression positively associates with poor prognoses for CRC patients

CTGF/CCN2 mediates tumor niche remodeling under PKR-activating ribosomal stress

CTGF/CCN2 antagonism of Wnt regulates cancer stemness and chemoresistance

Kim et al., iScience *23*, 101076
May 22, 2020
https://doi.org/10.1016/j.isci.2020.101076

iScience

CellPress
OPEN ACCESS

Article

Dynamic Malignant Wave of Ribosome-Insulted Gut Niche via the Wnt-CTGF/CCN2 Circuit

Ki Hyung Kim,[1,2,3,4] Seung Joon Lee,[1,4] Juil Kim,[1] and Yuseok Moon[1,3,5,*]

SUMMARY

Stress-driven ribosome dysfunction triggers an eIF2α-mediated integrated stress response to maintain cellular homeostasis. Among four key eIF2α kinases, protein kinase R (PKR) expression positively associates with poor prognoses for colorectal cancer (CRC) patients. We identified PKR-linked Wnt signaling networks that facilitate early inflammatory niche and epithelial-mesenchymal transitions of tumor tissues in response to ribosomal insults. However, the downstream Wnt signaling target fibrogenic connective tissue growth factor (CTGF/CCN2) regulates the nuclear translocation of β-catenin in a negative feedback manner. Moreover, dwindling expression of the Wnt/β-catenin pathway-regulator CTGF triggers noncanonical Wnt pathway-mediated exacerbation of intestinal cancer progression such as an increase in cancer stemness and acquisition of chemoresistance in the presence of ribosomal insults. The Wnt-CTGF-circuit-associated landscape of oncogenic signaling events was verified with clinical genomic profiling. This ribosome-associated wave of crosstalk between stress and oncogenes provides valuable insight into potential molecular interventions against intestinal malignancies.

INTRODUCTION

Colorectal cancer is an environmental disease primarily influenced by chronic epithelial stress in the gastrointestinal tract in combination with etiologies of genetic mutations (Huxley et al., 2009; Rattray et al., 2017). Germline mutations in the *adenomatous polyposis coli (APC)* tumor suppressor gene, which result in ectopic activation of Wnt/β-catenin signaling, and alterations of oncogenes including *KRAS*, *TP53*, and *EGFR* are leading causes of hereditary intestinal cancers (Armaghany et al., 2012). The noncanonical Wnt/planar cell polarity (PCP) signaling pathway is also involved in tumor initiation, progression, metastasis, and relapse (Daulat and Borg, 2017). Along with genetic mutations, the tumor microenvironment (niche) is crucial for progression to malignancy. In particular, tumor-associated inflammation is a hallmark of progression into metastatic stages via phenotypic change to tumor cells, with migratory and invasive properties emerging through the epithelial–mesenchymal transition (EMT). Stress-induced EMT is involved in the disruption of the tightly regulated intestinal epithelial layer and invasion, metastasis, and resistance to apoptosis during cancer progression. Inflammation is also a potent trigger of tumor EMT, and EMT programs can also stimulate the production of cancer-cell-derived proinflammatory mediators. These two events may thus mutually drive tumor cells toward malignancy.

In addition, EMT-mediated reprogramming of cell fate is a prerequisite for self-renewal and the cancer-initiation capacity of cancer stem cells (CSCs) (Pradella et al., 2017; Mani et al., 2008; Dave et al., 2012). EMT is relevant to the acquisition and maintenance of CSC-like properties, and CSCs often exhibit EMT-associated patterns (Liu and Fan, 2015; Singh and Settleman, 2010). These reciprocal features between EMT and CSCs have many implications for tumor progression. In addition, the EMT is an important point of convergence for inflammation and related pathogeneses, including fibrosis and cancer (Zhou et al., 2015a; Lopez-Novoa and Nieto, 2009). Fibrosis, resulting from failure of wound healing, shares similar patterns of progress with tumorigenesis (Rybinski et al., 2014), thus the fate of wound healing processes in response to gastrointestinal injuries may influence tumor progression and fibrotic developments. Many soluble and matrix elements forming the inflammatory wound microenvironment are present during both chronic fibrosis and tumor progression (Rybinski et al., 2014). One such component, connective tissue growth factor (CTGF), belongs to the cellular communication network factor (CCN) family of extracellular-matrix-associated heparin-binding proteins and is officially named as CCN2 (Perbal et al., 2018).

[1]Laboratory of Mucosal Exposome and Biomodulation, Department of Biomedical Sciences, Pusan National University, Yangsan 50612, Korea

[2]Department of Obstetrics and Gynecology, Pusan National University College of Medicine, Busan 49241, Korea

[3]Biomedical Research Institute, Pusan National University Hospital, Busan, 49241, Korea

[4]These authors contributed equally

[5]Lead contact

*Correspondence: moon@pnu.edu

https://doi.org/10.1016/j.isci.2020.101076

CTGF/CCN2 plays crucial roles in tissue remodeling during inflammation and fibrosis (Ramazani et al., 2018).

In response to internal or external stresses, including viral infection, cellular ribosomes act as sentinels. Stress-driven ribosomal dysfunction from ribosomal insults triggers eukaryotic translation initiation factor 2 subunit α (eIF2α)-mediated global translational inhibition via protein kinase R (PKR). This inhibition coincides with the induction of specific genes to enable cellular survival, eliminate severely injured cells, and boost innate immunity to viral infection, all of which are integrated stress responses (ISR) (He et al., 2012; Pakos-Zebrucka et al., 2016; Zhou et al., 2014). In addition to viral infection or specific translational inhibitors, ribosomal translation can be inhibited by internal or external stressors such as oxidative and ER stress, growth factor deprivation, or bacterial infection, which all lead to ISR via PKR activation (Pakos-Zebrucka et al., 2016; Williams, 1999; Spriggs et al., 2010; Steffen and Dillin, 2016; Sulima et al., 2017).

The ISR, along with other cellular adaptation pathways, plays a pivotal role in the cellular response to stress (Pakos-Zebrucka et al., 2016), primarily through global translational inhibition and the upregulation of pro-survival signaling. In the gastrointestinal tract, the ISR prevents injury of the intestinal barrier integrity by luminal insults. For instance, reparative inflammation in response to ribosomal insults helps maintain intestinal homeostasis (Vyleta et al., 2012; Park et al., 2012, 2013). In particular, anti-inflammatory responses and regenerative wound healing are important for mitigating tissue damage and controlling additional proinflammatory insults from gut microbial infections in the mucosa.

Discordant pathways of ribosomal-insult-associated ISR are potent etiological factors influencing epithelial inflammatory and chronic disorders including cancers (Mishra et al., 2016; Graziani et al., 2015; Yoder et al., 2007). In particular, the profiles of cytokines and growth factors are vigorously perturbed in the epithelia during translation misregulation, leading to mucosal inflammatory injuries and potent chronic outcomes. Repetitive instances of these aberrant responses and accumulated stress increase the risk of malignant mucosal disorders such as intestinal bowel disease (IBD), bowel fibrosis, and sporadic CRC (Speca et al., 2012; Lopez-Novoa and Nieto, 2009). Moreover, the misregulation of translation in cancer cell metabolism confirms the relevance of ribosomes for oncogenesis, and the recent discovery of somatic mutations in ribosomal proteins in several cancers strengthens the link between ribosomal defects and cancer progression (Sulima et al., 2017). Moreover, our recent investigation demonstrated that the ribosomal insult facilitates tumor-malignancy-associated features in CRC cells *in vitro* (Oh et al., 2016). In this study, we assumed that disorganization of the ribosomal-insult-associated ISR is a driving force for transformation of signaling network during CRC progression. In particular, tissue-remodeling-linked Wnt signaling was assessed as a potent mediator of malignant niche transformation during stress-driven ribosomal dysfunction.

RESULTS

CTGF/CCN2 Is Involved in PKR-Associated Inflammatory Signaling of the Wnt-Linked Tumor Niche under the Ribosomal Stress

Based on the assumption that the integrated stress responses (ISRs) may be involved in tumor progression, expression levels of four different global-stress-related mammalian eIF2α kinases, EIF2AK1, EIF2AK2, EIF2AK3, and EIF2AK4, were evaluated in CRC patients based on clinical genomic datasets (gse14333, n = 290) (Figure 1A). In particular, high expression levels of EIF2AK2 (PKR) are positively associated with bad prognoses for CRC patients.

The ribosome is a key intracellular sentinel for stress, and stress-driven ribosomal inactivation triggers eIF2α-mediated global translational inhibition via PKR (He et al., 2012; Pakos-Zebrucka et al., 2016; Zhou et al., 2014). The impacts of PKR-linked ISR on gut niche remodeling were examined in response to specific chemical ribosome-inactivating stress (RIS). Impacts of RIS-linked tissue remodeling on intestinal tumors were assessed in $APC^{min/+}$ mice, which are a model of human familial adenomatous polyposis (FAP) (Figure 1B). Untreated $APC^{min/+}$ mice developed spontaneous adenomas (Figure 1B, red arrow heads), and ribosomal insults increased adenoma occurrence rates with accompanying high-grade dysplasia (Figure 1B).

RIS-induced events are also associated with mucosal inflammatory disorders. To probe for a potential connection between ribosomal-insult-associated ISRs and tumorigenesis severity via impaired inflammation, we examined infiltrating macrophages in lesions of ribosome-insulted $APC^{min/+}$ mouse intestines.

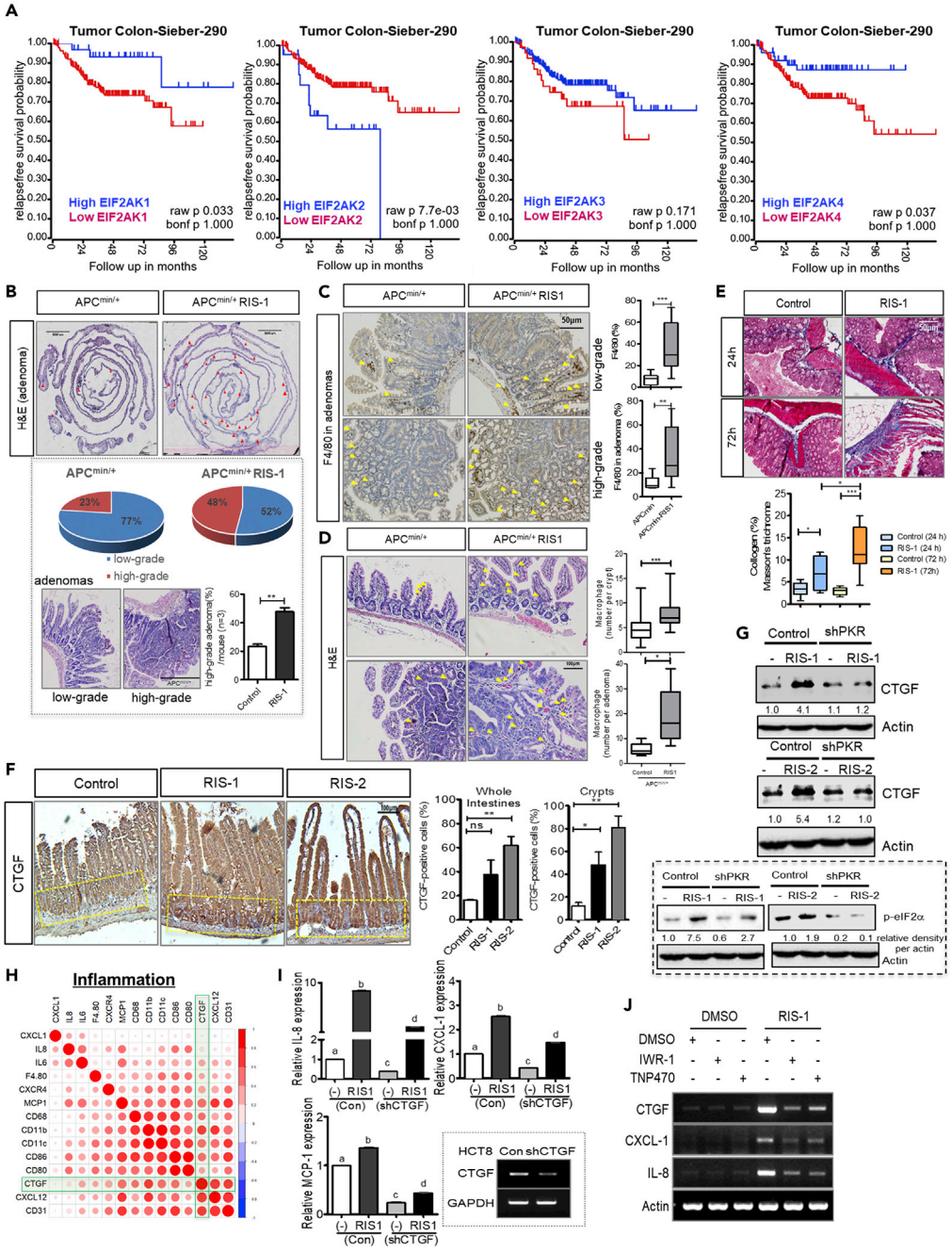

Figure 1. Roles of PKR Activation in the Intestinal Tumor Niche

(A) *Kaplan-Meier* plot of survival analysis based on tissue transcript levels in patients with CRC from *Sieber*'s dataset (left, GEO ID: gse14333, n = 290; high EIF2AK1 > 1391, n = 34; low EIF2AK1 < 1391, n = 192; high EIF2AK2 > 831.5, n = 21; low EIF2AK2 < 831.5, n = 205; high EIF2AK3 > 292.4, n = 189; low EIF2AK3 < 292.4, n = 37; high EIF2AK4 > 199.8, n = 53 low EIF2AK4 < 199.8, n = 173).

(B–D) (B) Hematoxylin and eosin staining of small intestines of $APC^{min/+}$ mice exposed to vehicle or RIS-1 (25 mg/kg) by oral gavage for 72 h. We counted phenotypically distinct polyps and adenomas (red arrow heads). Low- and high-grade dysplasias were subdivided based on hyperplastic features of crypts and villi. Results are shown as mean values ± SEM. (C and D) Immunohistochemistry with F4/80 (C) and hematoxylin/eosin staining (D) of tumor-associated macrophages in the small intestines of $APC^{min/+}$ mice exposed to vehicle or RIS-1 (25 mg/kg) for 72 h by oral gavage. F4/80-postive and both round-shaped and pink-colored macrophages were accumulated and ectopically dispersed in the lamina propria,

Figure 1. *Continued*

muscularis mucosa, and submucosa of the small intestines. The number of macrophages per crypt and adenoma were counted (right graphs). Results are shown as box-and-whisker plots (min to max).

(E) Trichrome staining of intestinal tissues of C57BL/6 mice treated with vehicle control or RIS-1(anisomycin) (25 mg/kg) for 24–72 h. Quantification and statistical analysis of connective tissues (lower graph). Results are shown as box-and-whisker plots (min to max).

(F) Immunocytochemistry with CTGF/CCN2 in intestines of C57BL/6 mice treated with either vehicle control or RIS-1 (25 mg/kg) for 72 h and statistical analysis of DAB-positive CTGF expression in total intestines and crypts (right graphs). Yellow dashed rectangles indicate the crypt region. Results are shown as mean values ±SEM.

(G) Control and PKR knockdown HCT8 cells were treated with 50 ng/mL RIS-1 (anisomycin) or 500 ng/mL RIS-2 (deoxynivalenol) for 1 h or 5 min (dashed box), then examined by western blotting.

(H) *Pearson*'s correlation analysis of relationships between transcription levels of CTGF and critical components of inflammation, EMT, and cancer stemness signaling pathways in CRC patients (TCGA-COAD, n = 440). Correlation matrix visualization generated using the corrplot function of the R-package (R Foundation for Statistical Computing, Vienna, Austria. URL: https://www.R-project.org/). Correlations of transcriptional expression among genes were interpreted according to a general guideline for Pearson's coefficient value: $r > 0.7$, high (+); $0.5 < r < 0.7$, moderate (+); $0.3 < r < 0.5$, moderate (+) or low (+); $0.1 < r < 0.3$, low (+); $-0.1 < r < 0.1$, negligible; $-0.3 < r < -0.1$, low (−).

(I) qRT-PCR of proinflammatory cytokines in control or CTGF-deficient (shCTGF-expressing) HCT8 cells after treatment with 50 ng/mL RIS-1 for 2 h. Transcript levels were normalized to those of the control. Results are shown as mean values ± SEM.

(J) Semi-quantitative RT-PCR with CTGF and proinflammatory cytokines. HCT116 cells were treated with either IWR-1 (30 μM) or TNP470 (100 μM) for 6 h prior to 1-h exposure to 50 ng/mL RIS-1.

Expression levels of F4/80, a macrophage marker, were ectopically increased (Figure 1C). The observed increases in pink-colored and round-shaped leukocytes in the $APC^{min/+}$ mouse intestines in response to ribosomal inactivation further confirms formation of the inflammatory tumor niche (Figure 1D).

Levels of connective tissue components, including collagen, were elevated in ribosome-insulted murine colons over time (Figure 1E), likely representing a dysregulated reparative inflammatory response. Moreover, enhanced expression of CTGF confirmed the presence of aggravated fibrogenic phenotypes in the guts of the same ribosome-insult mouse model (Figure 1F). In particular, intestinal pathogenesis triggered by ribosomal dysfunction was recapitulated in HCT8 cells, which are widely used as an enterocyte model for inflammatory and infectious diseases (Alcantara Warren et al., 2008; Thebault et al., 2006). Moreover, the ileocecum of the small intestine, the source of the HCT-8 cell line, is one of the most susceptible regions to ribosomal-dysfunction-associated ISR in the gastrointestinal tract (Avantaggiato et al., 2004; Obremski et al., 2008). Consistent with the occurrence of murine gut stress (Figures 1E and 1F), in human intestinal cells, transcript levels of CTGF, a fibrogenic marker, were significantly increased in response to chemical ribosomal inactivation in a dose-dependent manner (Figure S1A). Moreover, CTGF expression was highly dependent on PKR-linked pathway (Figure 1G), because PKR inhibition suppressed RIS-induced phosphorylation of eIF2α and CTGF expression (Figure 1G). In terms of inflammation, CTGF was positively associated with genes involved in chemokine signaling and actions in CRC patients based on clinical genomic dataset (TCGA-COAD) (Figure 1H). In association with CTGF/CCN2 induction, levels of the chemokines, including CXCL-1, MCP-1, and IL-8, were elevated in ribosome-insulted human intestinal cells, thus phenocopying early inflammatory responses (Figure S1B). Assessments of loss-of-function using shRNA expression showed that increased levels of proinflammatory cytokine transcripts are dependent on CTGF in the ribosome-insulted HCT8 (Figure 1I).

The involvement of Wnt signaling in chemokine expression was also evaluated, because $APC^{min/+}$ mice displayed elevated proinflammatory responses to ribosomal insults in the gut. Both Wnt/β-catenin and Wnt/PCP signaling were positively associated with ribosomal-dysfunction-induced increases in CTGF (Figures 1J and S1C) and chemokine levels *in vitro* (Figure 1J). Additionally, the promoter activity of IL-8 was attenuated in CTGF-knockdown cells (Figure S1D). Moreover, CTGF was positively involved in regulation of early growth response protein 1 (EGR1) and mitogen-activated kinases, which are well-known signaling mediators in chemokine induction in ribosome-insulted human intestinal cells (Figure S1E). Although CTGF positively regulates cytokine transcription, it negatively affects post-transcriptional regulation of cytokines in current culture-based models. Knockdown of CTGF also enhanced IL-8 mRNA stability and 3′UTR activity in human intestinal cells exposed to ribosomal insults (Figures S1F and S1G). Based on these ribosomal insult-induced chemokine and CTGF production, we hypothesize that stress-driven ribosomal dysfunction facilitates generation of early inflammatory and fibrogenic niches during tumorigenesis.

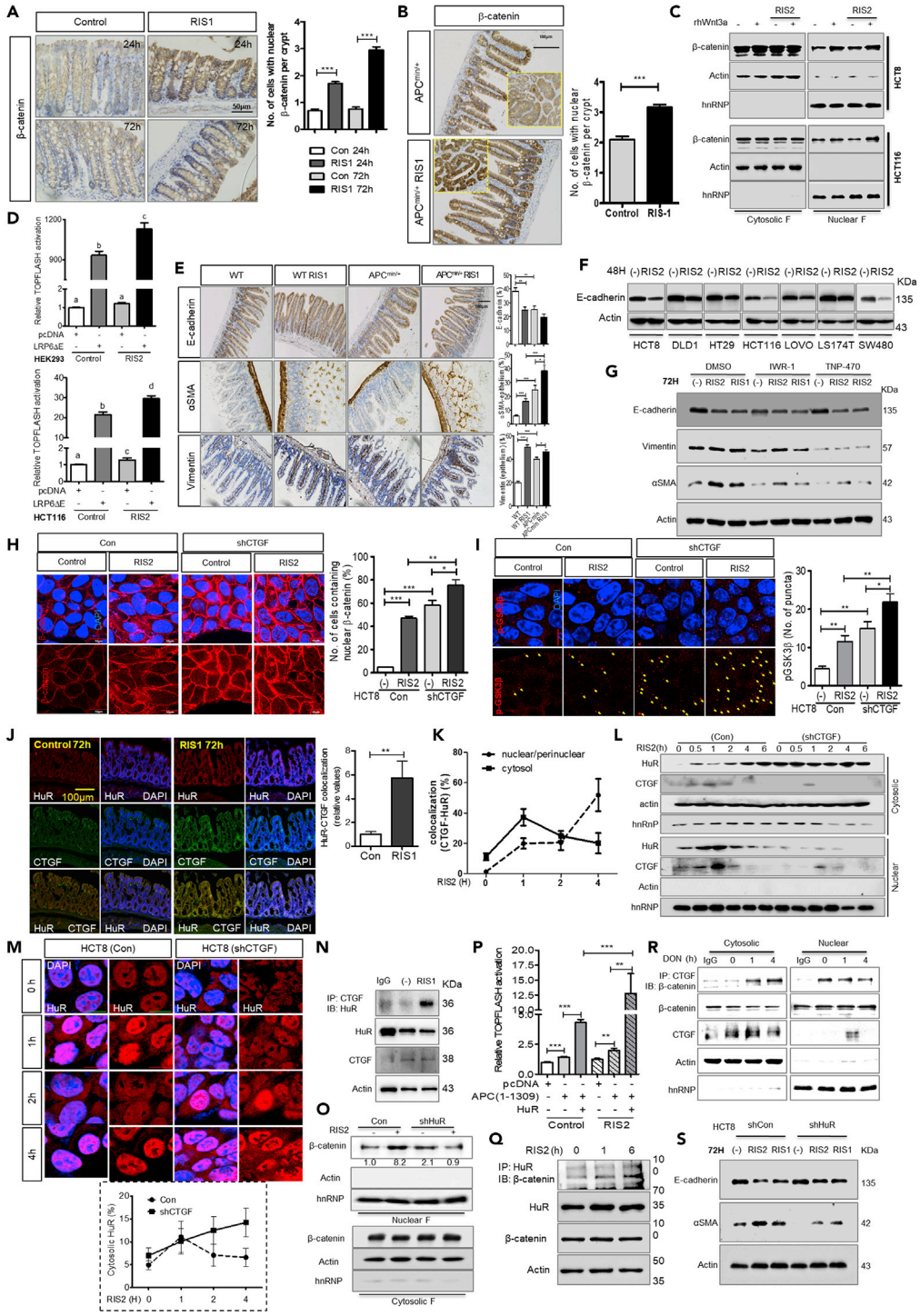

Figure 2. Effects of Ribosomal Insults on EMT in the Wnt-CTGF/CCN2 Axis

(A) IHC analysis of β-catenin in colonic tissues of C57BL/6 mice treated with either vehicle controls or RIS-1 (25 mg/kg) for 24–72 h with statistical quantification of nuclear accumulated β-catenin (right graph).

(B) Immunohistochemistry analysis of β-catenin in small intestines of $APC^{min/+}$ mice exposed to a vehicle control or RIS-1 (25 mg/kg) by oral gavage for 72 h. Yellow dashed rectangles are magnified views showing altered nuclear accumulation of β-catenin in the first row.

Figure 2. *Continued*

(C) HCT8 and HCT116 cells were treated with 500 ng/mL RIS-2 for 6 h during serum starvation prior to treatment with 100 ng/mL recombinant human Wnt3a (rhWnt3a) for 12 h and 1 h, respectively. To determine the level of activation of Wnt/β-catenin signaling, β-catenin levels were assessed in the nuclear fraction of cell lysates by Western blot.

(D) TOPFLASH of pcDNA- or LRP6ΔE-transfected HEK293 (upper graph) and HCT116 (lower graph) cells in response to 500 ng/mL RIS-2 treatment for 16 h.

(E) Immunohistochemistry of EMT markers in small intestines of wild type and $APC^{min/+}$ mice exposed to vehicle or RIS-1 (25 mg/kg) by oral gavage for 72 h.

(F) Various colorectal epithelial cancer cell lines were exposed to 500 ng/mL RIS-2 for 48 h. Total cell lysates were subjected to Western blot analysis.

(G) HCT8 cells were treated with RIS-2 (500 ng/mL) or RIS-1 (50 ng/mL) in the presence of either IWR-1 (30 μM) or TNP470 (100 μM) for 72 h. Cell lysates were examined by Western blotting of EMT markers. All quantifications of IHC were performed using HistoQuest software and statistically analyzed.

(H and I) Subcellular localization of β-catenin was assessed in control and CTGF-deficient HCT8 cells exposed to 500 ng/mL RIS-2 for 30 min. Co-localization of DAPI with β-catenin was statistically analyzed in both the entire cellular region and in the nucleus. Translocation of nuclear β-catenin was verified by Wnt activation (H). Punctate subcellular localization of p-GSK3β was assessed by immunostaining (I).

(J) HuR co-localization with CTGF in intestines of C57BL/6 mice treated with RIS-1 (25 mg/kg) for 72 h. Co-localization of HuR with CTGF was quantified using Image J software.

(K) Dynamic co-localization of HuR with CTGF in response to treatment with 500 ng/mL RIS-2. Co-localization of HuR with CTGF in the nucleus or cytosol was assessed and quantified. The nuclear region included the nuclei and perinuclear compartments.

(L) Assessment of cytosolic and nuclear HuR in response to 500 ng/mL RIS-2.

(M) Subcellular localization of HuR in response to treatment with 500 ng/mL RIS-2 for 1 h–4 h. Cytosolic HuR was quantified using ImageJ software.

(N) Co-immunoprecipitation of CTGF with HuR of HCT8 cells exposed to 50 ng/mL RIS-1 for either 1 h or 4 h.

(O and P) (O) Assessment of nuclear β-catenin levels as a readout for Wnt/β-catenin pathway activation in HuR-deficient HCT8 cells exposed to 500 ng/mL RIS-2 for 30 min. (P) TOPFLASH assays were performed in HCT8 cells transfected with either pcDNA, APC(1-1309), and/or HuR expression vectors and treated with RIS-2 (500 ng/mL) for 6 h.

(Q) HCT8 cells exposed to RIS-2 (500 ng/mL) were subjected to immunoprecipitation for HuR and β-catenin.

(R) Immunoprecipitation of CTGF with β-catenin in HCT-8 cells treated with 500 ng/mL RIS-2.

(S) Control and HuR-deficient HCT8 cells were treated with RIS-2 (500 ng/mL) or RIS-1 (50 ng/mL) for 72 h, then assessed for EMT by Western blotting. Results in all graphs are shown as mean values ± SEM. Asterisks represent statistically significant values (*$p < 0.05$, **$p < 0.01$, ***$p < 0.001$). Different letters over each box represent statistically significant differences among groups based on one-way ANOVA ($p < 0.05$).

Wnt Mediates EMT Programming in the Ribosome-Insulted Intestinal Cancer Cells

Our murine genetic model of human FAP contains a defect in APC, a negative regulator of β-catenin, resulting in elevated levels of β-catenin in gut epithelia of ribosome-insulted mice in a time-dependent manner (Figure 2A). Moreover, ribosomal inactivation enhanced levels of nuclear β-catenin in $APC^{min/+}$ mice (Figure 2B), indicating a link between the ribosome and Wnt-linked oncogenic signaling. Furthermore, ribosomal insults lead to the additive or synergistic activation of Wnt/β-catenin signaling in human intestinal cells with constitutive Wnt signaling activation by recombinant human Wnt 3a (Figure 2C) or expression of a constitutively active form of LRP6, LRP6ΔE (Davidson et al., 2005) (Figure 2D), as indicated by nuclear β-catenin accumulation and luciferase reporters driven by the TCF/LEF promoter (TOPFLSH), respectively. Based on these biochemical analyses, it was hypothesized that Wnt signaling induced by ribosomal insults may contribute to the severity of disease symptoms of APC mutant mice.

As a critical pathological feature of malignancy triggered by disturbances in Wnt signaling, EMT-mediated exacerbation of CRC was assessed in gut epithelium in response to ribosomal insult. First, to verify the relevance of ribosomal insults to exacerbation of adenoma via EMT, we examined alterations in expression levels of E-cadherin, αSMA, and vimentin. Reductions in E-cadherin levels and increases in αSMA and vimentin levels were consistently observed during EMT in the hereditary intestinal cancer model (Figure 2E). Moreover, these EMT-associated patterns displayed significantly elevated responses to ribosome-associated stress (Figures 2E and S2A). Notably, ectopic expression of αSMA in the intestinal epithelium indicates progression in cellular differentiation into adenocarcinomas in guts upon ribosomal insult (Figure 2E).

In addition to impacts on EMT in mice with hereditary intestinal cancer, human CRC cells showed suppressed levels of E-cadherin in response to ribosomal inactivation *in vitro* (Figure 2F). To reveal the underlying molecular mechanisms, we tested whether Wnt/β-catenin and Wnt/PCP signaling were involved in the

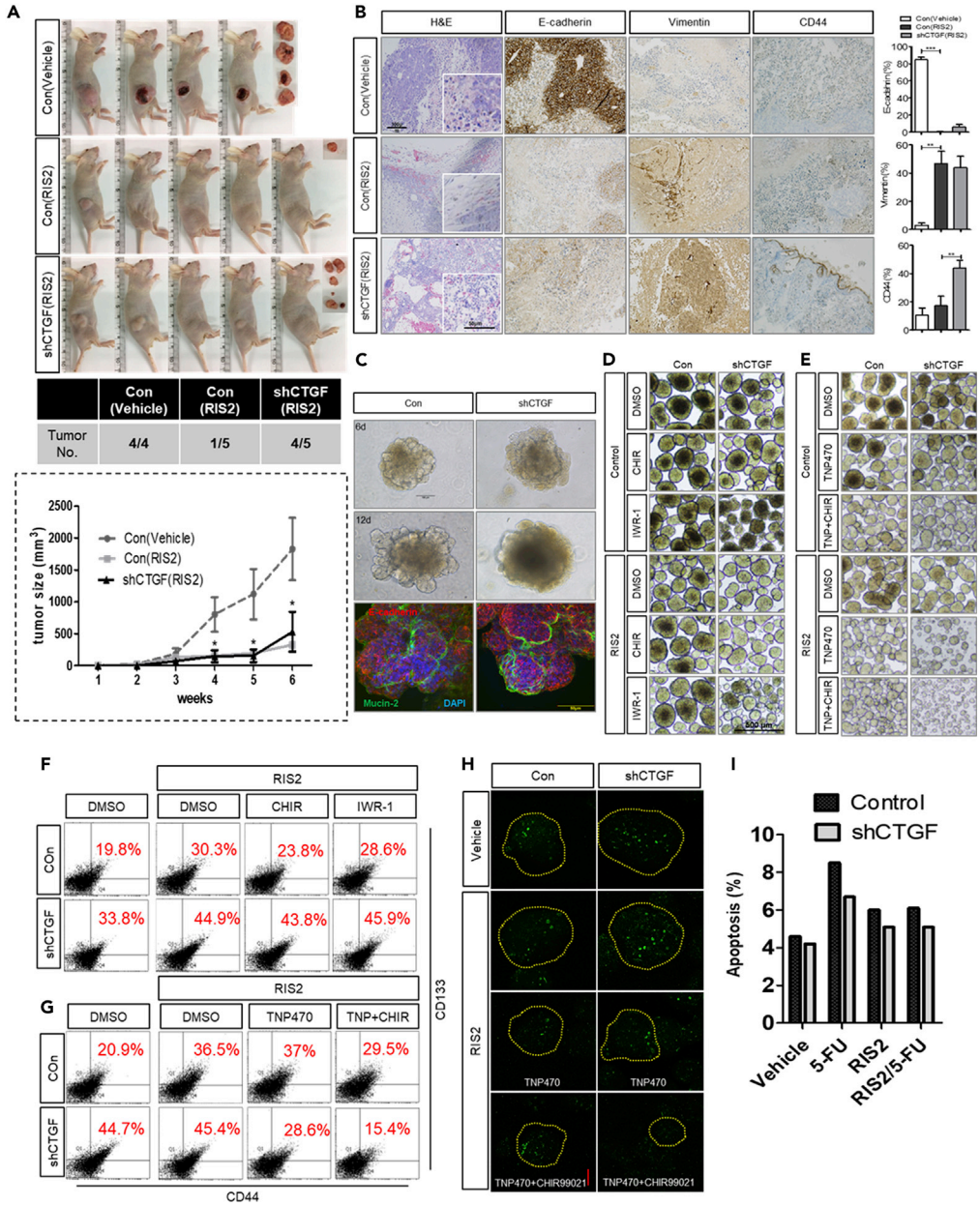

Figure 3. CTGF/CCN2 Suppression-Linked Stemness in CRC

(A) Xenograft assay of HCT8 colonospheres. Cultured spheroidal cells were dissociated into single cells and subcutaneously injected into the lateral flank region of SCID nude mice. Tumor occurrence and growth curves based on tumor volume measurements (lower panel and graph).

(B) Hematoxylin and eosin staining and immunohistochemistry of xenograft tumors targeting E-cadherin, vimentin, and CD44. Results are shown as mean values ± SEM. Asterisks represent statistically significant values (*$p < 0.05$, **$p < 0.01$, ***$p < 0.001$).

(C) Control and CTGF-deficient HCT8 cells exposed to RIS-2 were used to create CRC organoid cultures as described in the methods. CRC organoids were evaluated in terms of morphology (crypt formation), differentiation of epithelium (E-cadherin), and differentiated goblet cells (Mucin-2).

(D–H) Control and CTGF-deficient cells were exposed to 500 ng/mL of RIS-2 or 50 ng/mL of RIS-1 with other inhibitors for 24 h, then cultured to form spheres for 6 d. Colonosphere formation (D and E), flow cytometry of HCT8 spheroid cells with CD44-FITC and CD133-APC (F and G), immunostaining of HCT8 spheres with CD44-FITC, and analysis of CD44-positive cancer stemness using confocal microscopic Z-stacked images (H).

Figure 3. *Continued*
(I) Apoptosis of spheroidal cells as measured using propidium iodide (PI) and annexin V to assess sensitivity to cytotoxic 5-FU (375 μM) as described in the methods.

ribosomal dysfunction-induced alteration of EMT programs. EMT in ribosome-insulted CRC cells was hardly detectable when Wnt/β-catenin and Wnt/PCP signaling were blocked with the inhibitors IWR-1 endo or TNP470, respectively (Figure 2G). Taken together, these results indicate that Wnt signaling is involved in early transformation of tumor cells, including during the EMT process, in response to the ribosomal dysfunction.

Availability of Cytosolic HuR Determines Wnt-CTGF/CCN2 Circuit Activity in the Ribosome-Insulted Cells

In terms of signaling, because Wnt signaling was positively involved in CTGF expression (Figure 1J), blocking of CTGF enhanced levels of nuclear β-catenin and p-GSK3β in a negative feedback manner under the ribosomal insult (Figures 2H and 2I). To fully understand this negative circuit between CTGF and Wnt signaling, we sought to identify the nuclear translocation mechanism of β-catenin in our ribosomal insult model. Ribosomal dysfunction triggers the cytosolic translocation of HuR (human antigen R, ELAV-like protein 1) (Do et al., 2013, 2016), which post-transcriptionally regulates target mRNA by directly binding transcripts in AU-rich regions of their 3′UTRs, thus enhancing transcript stability (Matoulkova et al., 2012). In our model, co-localization of HuR and CTGF was significantly enhanced in mouse colons with ribosomal insults (Figure 2J). Quantification of cytosolic and perinuclear co-localization of CTGF and HuR in intestinal cancer cells with ribosomal insults revealed that cytosolic co-localization levels decreased while perinuclear co-localization increased with time (Figures 2K and S2B). Increase in cytosolic HuR in response to ribosomal insults was exacerbated by suppression of CTGF expression (Figure 2L), as supported by observations on HuR subcellular localization (Figure S1C). In CTGF-knockdown cells, HuR were resistant to returning to nuclei and remained in the cytosolic parts (Figure 2M), indicating regulatory interactions between CTGF and HuR in the nucleus. In addition, HuR physically interacts with CTGF in response to ribosomal dysfunction (Figure 2N). Taken together, these results suggest that CTGF inhibits trafficking of HuR to cytosol via physical protein interaction and confinement of translocation. Otherwise, free HuR would perform its own duty of mRNA stability regulation in the cytoplasm of cells.

Although ribosomal-insult-triggered HuR translocation mediates increases in proinflammatory cytokine via enhanced mRNA stability (Choi et al., 2009; Park et al., 2013), CTGF may counteract HuR function via physical interactions and modulation of HuR trafficking. This explanation is reasonably consistent with CTGF-mediated inhibition of IL-8 mRNA stability (Figures S1E and S1F), despite CTGF-dependent transcriptional activation in response to ribosomal dysfunction (Figure S1C). Additionally, CTGF-mediated negative regulation of HuR is consistently associated with Wnt signaling regulation. HuR depletion reduces nuclear β-catenin levels (Figure 2O), whereas CTGF deficiency increases levels of β-catenin and p-GSK3β (Figures 2H and 2I). In contrast, HuR overexpression enhanced activity of TCF/LEF promoter-driven luciferase reporters in cells exposed to ribosomal insults (Figure 2P). In addition, β-catenin binds HuR (Figure 2Q) and CTCF (Figure 2R). Moreover, HuR, a crucial mediator of the Wnt-CTGF circuit, positively associates with ribosomal-insult-triggered tumor cell EMT (Figure 2S). Taken together, these findings indicate that inhibitory interactions of CTGF with HuR are involved in CTGF-dependent negative regulation of Wnt/β-catenin signaling. Mechanistically, CTGF depletes the cytosolic pool of HuR, which is a crucial mediator of nuclear entry by β-catenin in intestinal cancer cells with ribosomal insults.

CTGF/CCN2 Antagonism of Wnt Regulates Cancer Stemness and Chemoresistance during the Ribosomal Stress

Because CTGF counteracts Wnt/β-catenin signaling in our model, it was hypothesized that CTGF suppression may elevate Wnt-associated tumor cell growth *in vivo*. Although ribosomal insults facilitated creation of the inflammatory niche and the EMT process in the tumor tissues, spheroidal tumor cells with a history of pulsed-inhibition of ribosome showed less tumor cell growth than intact tumors (Figure 3A). However, in CTGF-attenuated spheroidal cell-driven xenografts, tumor occurrence was enhanced compared with WT spheroid cells in response to ribosomal insult. Characterization of xenograft tumors revealed discrepancies between effective tumor growth and cancer stemness. Closer observations of tumor tissues from mice indicated that high levels of epithelial status were maintained in tumors from normal spheroids, which showed decreased vimentin expression and no CD44(+) CSCs (Figure 3B). In contrast, ribosomal insult promoted

complete E-cadherin loss and significant increases in vimentin levels, indicating substantial mesenchymal character of xenograft tumors (Figure 3B). Both highly epithelial and highly mesenchymal tumors lacked CD44 (+) stem-like cells. In contrast, CTGF-knockdown spheroid tumor tissues showed moderate EMT progress and significantly higher levels CD44 in response to the ribosomal insult (Figure 3B).

To further verify the role of CTGF reduction in exacerbation of colorectal tumor progression, we created tumor organoids using CSC-enriched intestinal cancer cells exposed to pulsed ribosomal inactivation. Normal CRC organoids showed multiple branches corresponding to enormous amounts of crypt-villus domains and relatively normal levels of E-cadherin and mucin-2. In contrast, CTGF-knockdown CRC organoids were round and compact with a lack of cryptic structure comparable to previously recapitulated tumor organoid (Sato et al., 2011), even though expression of E-cadherin and mucin-2 was ectopically enhanced (Figure 3C).

Next, we tried to address ribosomal-insult-associated triggering of CRC stemness in relation to the Wnt-CTGF signaling network. Spheroidal cultures of CRC cells after pulsed-inhibition of ribosomes were evaluated as *in vitro* cancer models to assess intratumoral heterogeneity and cancer stemness based on our previous report (Oh et al., 2016). Using these optimized colonosphere cultures in the presence of Wnt-specific inhibitors, Wnt/PCP signaling was proven necessary for spheroid formation (Figures 3D and 3E) and enhancement of CD44-and CD133-positive colon CSC populations when Wnt-regulating CTGF was suppressed (Figures 3F and 3G). Interestingly, ribosomal insult-induced increase in CD44(+)CD133(+) CSC populations was enhanced in CTGF-deficient cells, which was attenuated by TNP470-mediated ablation of Wnt/PCP signaling (Figure 3G). In addition, combined inhibition of Wnt/PCP and GSK3β signaling led to a significant loss of cancer stemness. These findings are supported by immunostaining of heterogeneously dispersed CD44 (+) colon CSCs in colonospheres (Figure 3H). Taken together, these results suggest that Wnt/PCP signaling dominantly contributes to colorectal cancer stemness and is prominent with decreased CTGF levels.

The spheroid-based evidence accounts for enhanced tumor stemness in CTGF-suppressed cells in our xenograft model. Moreover, the chemoresistance of ribosome-insulted spheroidal cells to 5-fluorouracil (5-FU), a first-line anti-cancer drug against CRC, reveals alterations in cancer stemness. Both annexin V and propidium iodide (PI)-positive apoptosis triggered by 5-FU were reduced in spheroids exposed to ribosomal insults. Moreover, CTGF depletion further attenuates 5-FU-induced cell death (Figure 3I), indicating a negative association between CTGF and chemoresistance of cancer spheroids.

The Non-canonical Wnt/PCP Pathway Mediates Cancer Stemness during Ribosomal Stress and in CRC Patients

Clinical transcriptomic analysis indicated that CRC patients with high levels of EIF2AK2 (PKR) as the key modulator of ribosomal insult responses have enhanced levels of signaling modules of the Wnt/PCP pathway, including RhoA GTPase and the Rho-associated kinase ROCK1 (Figure 4A). To verify the effect of ribosomal insults on Wnt/PCP signaling *in vivo*, we assessed expression levels of RhoA, a target gene of the PCP pathway in mouse intestines with ribosomal insults. Ribosomal insults increases levels of RhoA expression at comparable levels in both WT and $APC^{min/+}$ mouse intestines (Figure S3A). These trends were also observed in the colon (Figure S3B), with clear preferential expression of RhoA in epithelial crypts compared with the villus in mice with ribosomal insults (Figure 4B). Ribosomal insults also led to increased RhoA expression in severe adenomas of $APC^{min/+}$ mice (Figure 4C).

In response to ribosomal insults, levels of phospho-GSK3β (p-GSK3β), an inactive form of GSK3β indicating active Wnt/β-catenin signaling, were increased. Such increases were further enhanced in response to inhibition of Wnt/PCP signaling by TNP470. In contrast, levels of phospho-JNK (p-JNK), which indicate Wnt/PCP signaling activation (Kikuchi et al., 2009), were enhanced by inhibition of Wnt/β-catenin during ribosomal stress. Counteractions of Wnt/β-catenin and Wnt/PCP signaling were exaggerated in CTGF-depleted cells (Figure 4D).

The relationship between CTGF and Wnt signaling during ribosomal stress was similar to that in clinical expression profiles. We evaluated Pearson's correlation for transcript profiles of CTGF and Wnt-linked signaling pathways in CRC patients from the TCGA dataset (n = 440, COAD). In particular, levels of frizzled receptor-4 and -7, Wnt 5a, ROCK1, ROR2, and Prickled1 and 2, which are mainly involved in the Wnt/PCP

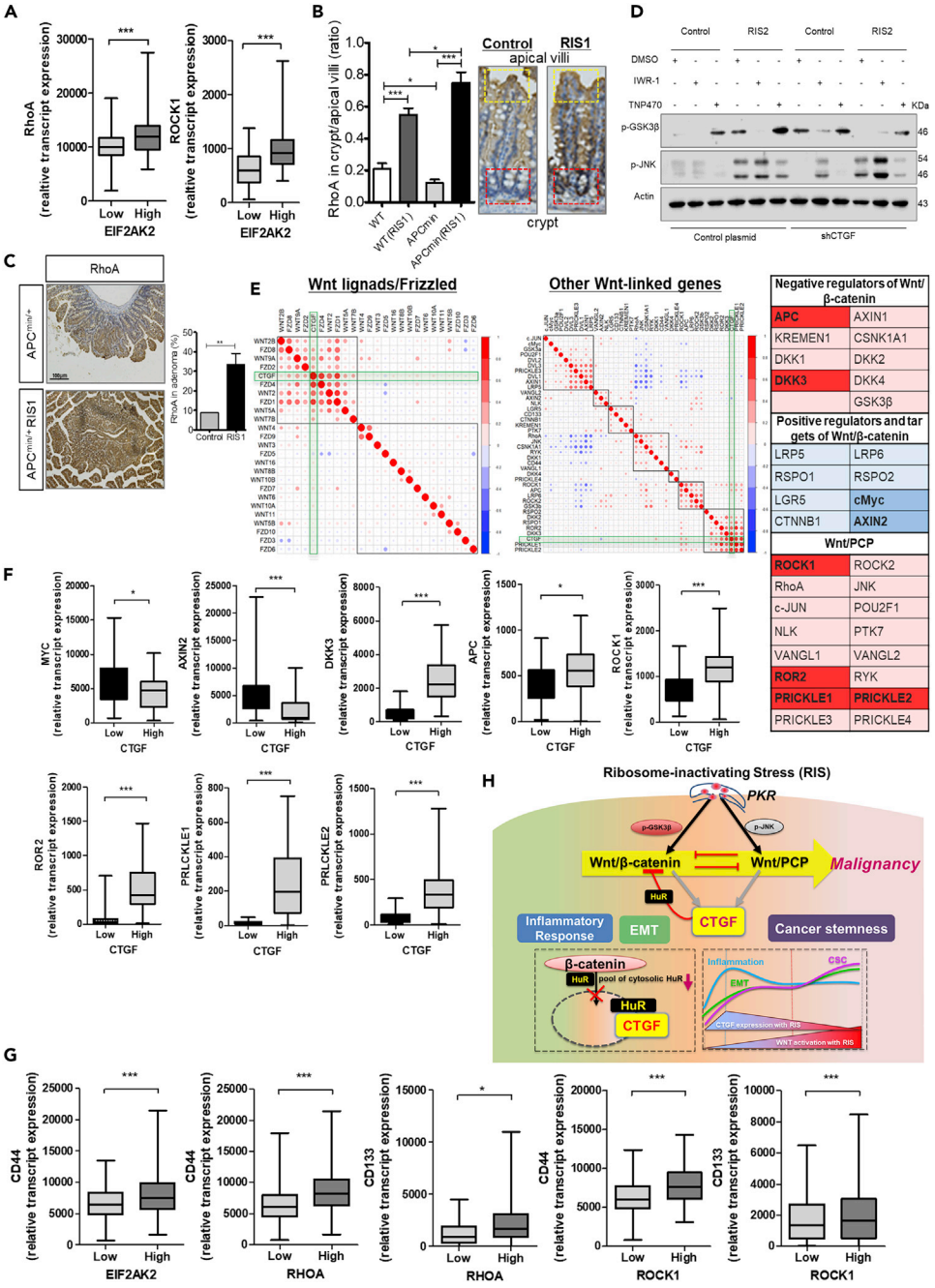

Negative regulators of Wnt/β-catenin	
APC	AXIN1
KREMEN1	CSNK1A1
DKK1	DKK2
DKK3	DKK4
	GSK3β
Positive regulators and tar gets of Wnt/β-catenin	
LRP5	LRP6
RSPO1	RSPO2
LGR5	cMyc
CTNNB1	AXIN2
Wnt/PCP	
ROCK1	ROCK2
RhoA	JNK
c-JUN	POU2F1
NLK	PTK7
VANGL1	VANGL2
ROR2	RYK
PRICKLE1	PRICKLE2
PRICKLE3	PRICKLE4

Figure 4. Wnt/PCP-Linked Cancer Cell Stemness in CRC

(A) Expression of Wnt/PCP-associated genes as assessed in CRC patients (TCGA-COAD, n = 440). Based on EIF2AK2 (PKR) levels, we chose the 100 highest and 100 lowest level samples, which were further compared for levels of RhoA (left) or ROCK1 (right). Results are shown as box-and-whisker plots (min to max). Asterisks (*) indicate significant differences from the low expression group ($p < 0.001$ ***).

(B and C) Intensity differences in RhoA between crypt and apical villi of small intestines of wild type and $APC^{min/+}$ mice exposed to vehicle or RIS-1 (25 mg/kg) by oral gavage for 72 h were assessed and statistically quantified. Representative staining of RhoA in wild-type mice (right). Immunohistochemistry of RhoA in adenomas (C). All immunohistochemical results were quantified using HistoQuest software based on the DAB-positive intensity of intestinal cells, then statistically analyzed. Results are shown as mean values ± SEM. Asterisks represent statistically significant values (*$p < 0.05$, **$p < 0.01$, ***$p < 0.001$).

Figure 4. *Continued*

(D) Western blot of p-GSK3β and p-JNK as a readout for activation of Wnt/β-catenin and Wnt/PCP signaling pathways, respectively, in the IWR-1 or TNP470-treated controls and CTGF-deficient HCT8 cells in response to treatment with 500 ng/mL RIS-2.

(E) Pearson's correlation analysis of transcriptional expression between CTGF and critical components, including Wnt signaling pathways, in CRC patients (TCGA-COAD, n = 440). Visualization of correlation matrix by corrplot of the R-package (R Foundation for Statistical Computing, Vienna, Austria. URL: https://www.R-project.org/). Genes with expression levels significantly correlated with CTGF in terms of paralogues of Wnts, frizzled receptors, and pivotal Wnt signaling components. Color gradients represent the degree of correlation with selected Wnt signaling components. Correlation of transcriptional expression among genes was interpreted according to a general guideline of Pearson coefficient values: $r > 0.7$, high (+); $0.5 < r < 0.7$, moderate (+); $0.3 < r < 0.5$, moderate (+) or low (+); $0.1 < r < 0.3$, low (+); $-0.1 < r < 0.1$, negligible; $-0.3 < r < -0.1$, low (−). Correlation patterns were visualized using corrplot of the R-package. Rectangles represent significantly correlated gene clusters.

(F and G) Expression of Wnt-associated genes (F) and cancer stemness markers (G) were assessed in CRC patients (TCGA-COAD, n = 440). Based on CTGF (F), EIF2AK2 (G), RHOA (G), or ROCK1 (G) levels, we chose the 100 highest and 100 lowest level samples, which were further evaluated based on CD44 or CD133 levels. Results are shown as box-and-whisker plots (min to max). Asterisks (*) indicate significant differences from the low expression group (*$p < 0.05$, **$p < 0.01$, ***$p < 0.001$).

(H) A working proposed dynamic wave model of the Wnt-CTGF axis in ribosomal-insult-associated CRC progression.

signaling pathways, were positively associated with CTGF levels (Figure 4E). In line with these findings, expression of APC and Dickkopf3 (DKK3), which are involved in attenuation of Wnt/β-catenin signaling, was positively associated with CTGF expression. In contrast, CTGF was negatively linked to Wnt/β-catenin signaling in the clinical dataset, which is consistent with protein levels in intestinal cancer cells. Moreover, CRC patients with high levels of CTGF displayed high expression levels of Wnt/β-catenin negative regulators (DKK3, APC) and Wnt/PCP signaling mediators (ROCK1, ROR2, PRLCKLE1/2) and low expression of Wnt/β-catenin positive regulators (MYC and AXIN2) (Figure 4F). In particular, patients with high levels of Wnt/PCP signaling mediators tend to show elevated expression levels of cancer-stemness-linked biomarkers (CD44 and CD133) (Figure 4G). Taken together, PKR-linked insults elevated cancer cell stemness, which was positively associated with Wnt/PCP signaling pathways and dwindling expression of CTGF.

DISCUSSION

In this study, we proposed that a PKR-activating ribosomal insult drives early remodeling of cell signaling, leading to alterations of intrinsic cancer competence and malignant microenvironments, although the ribosomal insult itself does not contribute to tumor cell proliferation. Mechanistically, the network including Wnt and CTGF/CCN2 plays crucial roles in phase-dependent regulation of inflammatory signaling, EMT programs, and cancer stemness via fine-tuning the balance between the Wnt/β-catenin and Wnt/PCP signaling pathways (Figure 4H). Unveiling molecular events in the Wnt-CTGF signaling network will advance our understanding of ribosomal-inactivation-mediated CRC progression, providing novel insights for interventions against CRC.

The eIF2α-mediated ISR is the primary cellular management method for maintaining homeostasis during ER and ribosomal stress. In particular, ribosomal-sentinel-associated proteins are closely involved in stem cell differentiation and regulation of oncogenic and tumor-suppressing genes (Sulima et al., 2017; Zhou et al., 2015b). Functional inactivation of the ribosome in our study triggered induction of CTGF and proinflammatory chemokine expression, which phenocopies early inflammatory responses during curative or reparative inflammation in oncogenesis. Within the mechanistic model proposed by this study, modulation of Wnt-CTGF signaling also contributed to immunity-associated microenvironments through regulation of cancer chemokines and macrophage infiltration.

Tumor-associated macrophages (TAMs) are potent mediators of cancer cell niche remodeling that promote metastasis, stimulating angiogenesis and evasion from T-cell-mediated immune surveillance by tumors (Grivennikov et al., 2010; Qian and Pollard, 2010). TAMs release various cytokines to exacerbate tumor progression, thus enhancing angiogenesis, invasion, and dissemination, which are closely linked to the EMT. In particular, the autocrine CXCR4-CXCL12 axis enhances differentiation of monocytes into macrophages and provides a pre-metastatic niche for cancer cells (Zhang et al., 2013; Qian et al., 2011). High correlation between CXCL12 and CTGF levels in gene expression profiles of CRC patients therefore indicates an important role for CTGF in immunity-related metastasis and EMT programming. In the present model, CTGF acts on both Wnt/β-catenin and Wnt/PCP signaling as a balancing node, thus regulating cancer-associated inflammation, EMT, immunity, and malignancy. Understanding regulatory mechanisms of ribosomal-insult-derived inflammation and associated events via the Wnt-CTGF axis will thus provide compelling therapeutic strategies targeting the progression of sporadic CRC.

The Wnt-CTGF/CCN2 axis is precisely modulated by the cytosolic availability of HuR during ribosomal stress. In particular, the cytoplasmic translocation of HuR is a hallmark of cellular ribosomal dysfunction and contributes to stabilization of the 3′-UTR-containing transcripts, including those of pro-inflammatory cytokines. The involvement of HuR in Wnt signaling has also previously been demonstrated. For instance, mTOR-activated heat shock factor 1 induces HuR expression, which then stabilizes and enhances the translation of β-catenin mRNAs in cancer cells (Lopez de Silanes et al., 2003; Chou et al., 2015). In addition, mRNAs encoding the Wnt receptor Lrp6 are stabilized by HuR. Knockdown of HuR therefore significantly decreases β-catenin mRNA levels (Ale-Agha et al., 2009). However, our study indicates novel functions of HuR other than the stabilization of Wnt-linked transcripts in intestinal cancer cells. Ribosomal insults trigger cytosolic translocation of HuR, which interacts with β-catenin and CTGF proteins instead of stabilizing their mRNA. CTGF-mediated inhibitory interactions with HuR exhaust the pool of HuR available for interaction with β-catenin in the cytoplasm. Without such depletion, CTCF-free HuR would facilitate the trafficking of β-catenin into nuclei as a transcription factor in tumor cells.

Experimental evidence of involvement of the Wnt-CTGF/CCN2 axis in ribosomal-insult-associated gastrointestinal pathogenesis is also supported by clinical patient profiles. Wnt signaling, which plays important roles in embryonic development, cellular homeostasis, and various types of carcinogenesis (Clevers, 2006), is subdivided into β-catenin-dependent planar cell polarity (PCP) and Wnt/Ca^{2+} signaling pathways. Oncogenic Wnt/β-catenin signaling is involved in tumor outgrowth, cancer cell metastasis, immunity, chemoresistance, and maintenance of CSCs (Vermeulen et al., 2010). Furthermore, the Wnt/PCP signaling pathway is related to the initiation, progression, metastasis, and relapse of cancer (Daulat and Borg, 2017). Wnt signaling is also critical for cancer-associated inflammation, immunity, EMT, and other forms of cancer malignancy in terms of oncogenic and cancer-supportive niches. β-catenin-dependent or -independent Wnt pathways play distinct roles via various combinatory interactions with ~19 Wnt ligands, ~10 paralogues of frizzled receptors, and co-receptors including LRP5/6 and receptor tyrosine kinase-like orphan receptor (ROR) 1/2.

Information about agonists or antagonists of Wnt and other related signaling pathways have extended our understanding of crosstalk and mechanisms enabling minute balancing between Wnt/β-catenin and Wnt/PCP signaling, enhancing knowledge of cancer biology and the identification of effective therapeutic targets. In our study, CTGF appears to represent a convergent point between Wnt/β-catenin and Wnt/PCP signaling. Wnt/β-catenin signaling is responsible for the maintenance of cancer stemness and growth of colon spheroidal cells (Vermeulen et al., 2010; Kanwar et al., 2010). The observation of endogenously negative effects of CTGF on Wnt/β-catenin signaling corroborates increases of CD44-positive cancer stem cell populations in the absence of CTGF due to activation of Wnt/β-catenin signaling. We also found that Wnt/PCP signaling is critical to acquisition of ribosomal-inactivation-induced cancer stemness. Moreover, activation of the RhoA-ROCK axis is essential to Wnt/PCP signaling, and RhoA signaling is necessary to maintain adherens junctions and cellular migration in normal intestinal epithelia and colorectal cancer (Sahai and Marshall, 2002). In our study, RhoA expression was significantly elevated in guts exposed to ribosomal insults, and the specific local distribution of RhoA in the progenitor-rich distal crypts of the small intestines was prominent (Figure 3H).

CTGF/CCN2 can also interact with the extracellular domain of LRP6, thus negatively regulating LRP6-mediated Wnt activation. Consistent with this relationship, our data demonstrated that a CTGF-binding-site-deficient LRP6ΔE, a constitutively active LRP6 lacking most of its extracellular domain, enhances Wnt signaling and the induction of Wnt-associated EMT (Figure 2D). Moreover, because both non-canonical and canonical Wnt signaling are required for CTGF expression (Figure 1J), negative feedback regulation of Wnt signaling by CTGF can be inferred. Even though cancer stemness was increased in response to ribosomal inactivation, tumor growth was impaired because of high amounts of transition to the mesenchymal state. However, compared with wild-type CRC cell spheroid-originating organoids, cryptic integrity was disrupted in CTGF-deficient tumor organoids, contributing to the malignant alteration of tumor microenvironments, high increases in the CD44-positive cancer stem cell populations, and attenuation of sensitivity to an anti-cancer drug. These results suggest that phase-dependent regulation of CTGF is crucial to the malignancy of latent competent cancer cells via an imbalance in Wnt signaling, although the growth of ribosome-insulted cancer cells is decreased. Even though the latent relapse is a major concern in cancer clinics, little is known about the nature of dormant cancer cells and the latency mechanisms allowing these cells to remain quiescent, evade immunity, retain tumor-initiating capacity, and evolve aggressive metastatic features (Malladi et al., 2016). Our investigations of stress-associated malignant shifts of tumor niches thus provide novel insight into early transformation and latency-related features of the progression and relapse of CRC related to the signaling waves of the Wnt-CTGF axis.

limitations of the study

A few limitations should be considered when interpreting our data. Although we identified malignancy-related signaling networks in ribosome-insulted cancer cells, it will be of interest to assess further if these are generated directly in patients with chemoresistant CRC. In addition, the computational modeling with extensive experimental datasets would contribute to better understanding of the adverse outcome pathways in sporadic CRC.

METHODS

All methods can be found in the accompanying Transparent Methods supplemental file.

DATA AND CODE AVAILABILITY

All relevant data are available from the authors upon request.

SUPPLEMENTAL INFORMATION

Supplemental Information can be found online at https://doi.org/10.1016/j.isci.2020.101076.

ACKNOWLEDGMENTS

This research was supported by the Basic Science Research Program through the National Research Foundation of Korea (NRF) funded by the Ministry of Education (2018R1D1A3B05041889) and Ministry of Science and ICT (NRF-2019R1A2C1084827).

AUTHOR CONTRIBUTIONS

YM performed project design and hypotheses. JK, KHK, and SJL conducted experiments and analyzed experimental data. KHK performed the computational analyses of the clinical datasets. YM prepared the manuscript and supervised the overall project.

DECLARATION OF INTERESTS

The authors have no conflicts of interest to disclose.

Received: November 22, 2019
Revised: December 13, 2019
Accepted: April 14, 2020
Published: May 22, 2020

REFERENCES

Alcantara Warren, C., Destura, R.V., Sevilleja, J.E., Barroso, L.F., Carvalho, H., Barrett, L.J., O'Brien, A.D., and Guerrant, R.L. (2008). Detection of epithelial-cell injury, and quantification of infection, in the HCT-8 organoid model of cryptosporidiosis. J.Infect. Dis. *198*, 143–149.

Ale-Agha, N., Galban, S., Sobieroy, C., Abdelmohsen, K., Gorospe, M., Sies, H., and Klotz, L.O. (2009). HuR regulates gap junctional intercellular communication by controlling beta-catenin levels and adherens junction integrity. Hepatology *50*, 1567–1576.

Armaghany, T., Wilson, J.D., Chu, Q., and Mills, G. (2012). Genetic alterations in colorectal cancer. Gastrointest. Cancer Res. *5*, 19–27.

Avantaggiato, G., Havenaar, R., and Visconti, A. (2004). Evaluation of the intestinal absorption of deoxynivalenol and nivalenol by an in vitro gastrointestinal model, and the binding efficacy of activated carbon and other adsorbent materials. Food Chem. Toxicol. *42*, 817–824.

Choi, H.J., Yang, H., Park, S.H., and Moon, Y. (2009). HuR/ELAVL1 RNA binding protein modulates interleukin-8 induction by muco-active ribotoxin deoxynivalenol. Toxicol. Appl. Pharmacol. *240*, 46–54.

Chou, S.D., Murshid, A., Eguchi, T., Gong, J., and Calderwood, S.K. (2015). HSF1 regulation of beta-catenin in mammary cancer cells through control of HuR/elavL1 expression. Oncogene *34*, 2178–2188.

Clevers, H. (2006). Wnt/beta-catenin signaling in development and disease. Cell *127*, 469–480.

Daulat, A.M., and Borg, J.P. (2017). Wnt/planar cell polarity signaling: new opportunities for cancer treatment. Trends Cancer *3*, 113–125.

Dave, B., Mittal, V., Tan, N.M., and Chang, J.C. (2012). Epithelial-mesenchymal transition, cancer stem cells and treatment resistance. Breast Cancer Res. *14*, 202.

Davidson, G., Wu, W., Shen, J., Bilic, J., Fenger, U., Stannek, P., Glinka, A., and Niehrs, C. (2005). Casein kinase 1 gamma couples Wnt receptor activation to cytoplasmic signal transduction. Nature *438*, 867–872.

Do, K.H., Choi, H.J., Kim, J., Park, S.H., Kim, K.H., and Moon, Y. (2013). SOCS3 regulates BAFF in human enterocytes under ribosomal stress. J. Immunol. *190*, 6501–6510.

Do, K.H., Park, S.H., Kim, J., Yu, M., and Moon, Y. (2016). Ribosome inactivation leads to attenuation of intestinal polymeric Ig receptor expression via differential regulation of human antigen R. J. Immunol. *197*, 847–858.

Graziani, F., Pujol, A., Nicoletti, C., Pinton, P., Armand, L., Di Pasquale, E., Oswald, I.P., Perrier, J., and Maresca, M. (2015). The food-associated ribotoxin deoxynivalenol modulates inducible NO synthase in human intestinal cell model. Toxicol. Sci. *145*, 372–382.

Grivennikov, S.I., Greten, F.R., and Karin, M. (2010). Immunity, inflammation, and cancer. Cell *140*, 883–899.

He, K., Zhou, H.R., and Pestka, J.J. (2012). Mechanisms for ribotoxin-induced ribosomal RNA cleavage. Toxicol. Appl. Pharmacol. *265*, 10–18.

Huxley, R.R., Ansary-Moghaddam, A., Clifton, P., Czernichow, S., Parr, C.L., and Woodward, M. (2009). The impact of dietary and lifestyle risk factors on risk of colorectal cancer: a quantitative overview of the epidemiological evidence. Int. J. Cancer *125*, 171–180.

Kanwar, S.S., Yu, Y., Nautiyal, J., Patel, B.B., and Majumdar, A.P. (2010). The Wnt/beta-catenin pathway regulates growth and maintenance of colonospheres. Mol. Cancer *9*, 212.

Kikuchi, A., Yamamoto, H., and Sato, A. (2009). Selective activation mechanisms of Wnt signaling pathways. Trends Cell Biol. *19*, 119–129.

Liu, X., and Fan, D. (2015). The epithelial-mesenchymal transition and cancer stem cells: functional and mechanistic links. Curr. Pharm. Des. *21*, 1279–1291.

Lopez-Novoa, J.M., and Nieto, M.A. (2009). Inflammation and EMT: an alliance towards organ fibrosis and cancer progression. EMBO Mol. Med. *1*, 303–314.

Lopez de Silanes, I., Fan, J., Yang, X., Zonderman, A.B., Potapova, O., Pizer, E.S., and Gorospe, M. (2003). Role of the RNA-binding protein HuR in colon carcinogenesis. Oncogene *22*, 7146–7154.

Malladi, S., Macalinao, D.G., Jin, X., He, L., Basnet, H., Zou, Y., de Stanchina, E., and Massague, J. (2016). Metastatic latency and immune evasion through autocrine inhibition of WNT. Cell *165*, 45–60.

Mani, S.A., Guo, W., Liao, M.J., Eaton, E.N., Ayyanan, A., Zhou, A.Y., Brooks, M., Reinhard, F., Zhang, C.C., et al. (2008). The epithelial-mesenchymal transition generates cells with properties of stem cells. Cell *133*, 704–715.

Matoulkova, E., Michalova, E., Vojtesek, B., and Hrstka, R. (2012). The role of the 3' untranslated region in post-transcriptional regulation of protein expression in mammalian cells. RNA Biol. *9*, 563–576.

Mishra, S., Tewari, P., Chaudhari, B.P., Dwivedi, P.D., Pandey, H.P., and Das, M. (2016). Deoxynivalenol induced mouse skin tumor initiation: elucidation of molecular mechanisms in human HaCaT keratinocytes. Int. J. Cancer *139*, 2033–2046.

Obremski, K., Zielonka, L., Gajecka, M., Jakimiuk, E., Bakula, T., Baranowski, M., and Gajecki, M. (2008). Histological estimation of the small intestine wall after administration of feed containing deoxynivalenol, T-2 toxin and zearalenone in the pig. Pol. J. Vet. Sci. *11*, 339–345.

Oh, C.K., Lee, S.J., Park, S.H., and Moon, Y. (2016). Acquisition of chemoresistance and other malignancy-related features of colorectal cancer cells are incremented by ribosome-inactivating stress. J. Biol. Chem. *291*, 10173–10183.

Pakos-Zebrucka, K., Koryga, I., Mnich, K., Ljujic, M., Samali, A., and Gorman, A.M. (2016). The integrated stress response. EMBO Rep. *17*, 1374–1395.

Park, S.H., Choi, H.J., Do, K.H., Yang, H., Kim, J., and Moon, Y. (2012). Chronic Nod2 stimulation potentiates activating transcription factor 3 and paradoxical superinduction of epithelial proinflammatory chemokines by mucoactive ribotoxic stressors via RNA-binding protein human antigen R. Toxicol. Sci. *125*, 116–125.

Park, S.H., Do, K.H., Choi, H.J., Kim, J., Kim, K.H., Park, J., Oh, C.G., and Moon, Y. (2013). Novel regulatory action of ribosomal inactivation on epithelial Nod2-linked proinflammatory signals in two convergent ATF3-associated pathways. J. Immunol. *191*, 5170–5181.

Perbal, B., Tweedie, S., and Bruford, E. (2018). The official unified nomenclature adopted by the HGNC calls for the use of the acronyms, CCN1-6, and discontinuation in the use of CYR61, CTGF, NOV and WISP 1-3 respectively. J.Cell Commun.Signal. *12*, 625–629.

Pradella, D., Naro, C., Sette, C., and Ghigna, C. (2017). EMT and stemness: flexible processes tuned by alternative splicing in development and cancer progression. Mol. Cancer *16*, 8.

Qian, B.Z., Li, J., Zhang, H., Kitamura, T., Zhang, J., Campion, L.R., Kaiser, E.A., Snyder, L.A., and Pollard, J.W. (2011). CCL2 recruits inflammatory monocytes to facilitate breast-tumour metastasis. Nature *475*, 222–225.

Qian, B.Z., and Pollard, J.W. (2010). Macrophage diversity enhances tumor progression and metastasis. Cell *141*, 39–51.

Ramazani, Y., Knops, N., Elmonem, M.A., Nguyen, T.Q., Arcolino, F.O., van den Heuvel, L., Levtchenko, E., Kuypers, D., and Goldschmeding, R. (2018). Connective tissue growth factor (CTGF) from basics to clinics. Matrix Biol. *68-69*, 44–66.

Rattray, N.J.W., Charkoftaki, G., Rattray, Z., Hansen, J.E., Vasiliou, V., and Johnson, C.H. (2017). Environmental influences in the etiology of colorectal cancer: the premise of metabolomics. Curr.Pharmacol. Rep. *3*, 114–125.

Rybinski, B., Franco-Barraza, J., and Cukierman, E. (2014). The wound healing, chronic fibrosis, and cancer progression triad. Physiol. Genomics *46*, 223–244.

Sahai, E., and Marshall, C.J. (2002). ROCK and Dia have opposing effects on adherens junctions downstream of Rho. Nat.Cell Biol *4*, 408–415.

Sato, T., Stange, D.E., Ferrante, M., Vries, R.G., Van Es, J.H., Van den Brink, S., Van Houdt, W.J., Pronk, A., Van Gorp, J., et al. (2011). Long-term expansion of epithelial organoids from human colon, adenoma, adenocarcinoma, and Barrett's epithelium. Gastroenterology *141*, 1762–1772.

Singh, A., and Settleman, J. (2010). EMT, cancer stem cells and drug resistance: an emerging axis of evil in the war on cancer. Oncogene *29*, 4741–4751.

Speca, S., Giusti, I., Rieder, F., and Latella, G. (2012). Cellular and molecular mechanisms of intestinal fibrosis. World J. Gastroenterol. *18*, 3635–3661.

Spriggs, K.A., Bushell, M., and Willis, A.E. (2010). Translational regulation of gene expression during conditions of cell stress. Mol.Cell *40*, 228–237.

Steffen, K.K., and Dillin, A. (2016). A ribosomal perspective on proteostasis and aging. Cell Metab. *23*, 1004–1012.

Sulima, S.O., Hofman, I.J.F., De Keersmaecker, K., and Dinman, J.D. (2017). How ribosomes translate cancer. Cancer Discov. *7*, 1069–1087.

Thebault, S., Deniel, N., Marion, R., Charlionet, R., Tron, F., Cosquer, D., Leprince, J., Vaudry, H., Ducrotte, P., et al. (2006). Proteomic analysis of glutamine-treated human intestinal epithelial HCT-8 cells under basal and inflammatory conditions. Proteomics *6*, 3926–3937.

Vermeulen, L., De Sousa, E.M.F., van der Heijden, M., Cameron, K., de Jong, J.H., Borovski, T., Tuynman, J.B., Todaro, M., Merz, C., Rodermond, H., et al. (2010). Wnt activity defines colon cancer stem cells and is regulated by the microenvironment. Nat.Cell Biol. *12*, 468–476.

Vyleta, M.L., Wong, J., and Magun, B.E. (2012). Suppression of ribosomal function triggers innate immune signaling through activation of the NLRP3 inflammasome. PLoS One *7*, e36044.

Williams, B.R. (1999). PKR; a sentinel kinase for cellular stress. Oncogene *18*, 6112–6120.

Yoder, J.M., Aslam, R.U., and Mantis, N.J. (2007). Evidence for widespread epithelial damage and coincident production of monocyte chemotactic protein 1 in a murine model of intestinal ricin intoxication. Infect. Immun. *75*, 1745–1750.

Zhang, X.H., Jin, X., Malladi, S., Zou, Y., Wen, Y.H., Brogi, E., Smid, M., Foekens, J.A., and Massague, J. (2013). Selection of bone metastasis seeds by mesenchymal signals in the primary tumor stroma. Cell *154*, 1060–1073.

Zhou, H.R., He, K., Landgraf, J., Pan, X., and Pestka, J.J. (2014). Direct activation of ribosome-associated double-stranded RNA-dependent protein kinase (PKR) by deoxynivalenol, anisomycin and ricin: a new model for ribotoxic stress response induction. Toxins (Basel) *6*, 3406–3425.

Zhou, S.L., Zhou, Z.J., Hu, Z.Q., Li, X., Huang, X.W., Wang, Z., Fan, J., Dai, Z., and Zhou, J. (2015a). CXCR2/CXCL5 axis contributes to epithelial-mesenchymal transition of HCC cells through activating PI3K/Akt/GSK-3beta/Snail signaling. Cancer Lett. *358*, 124–135.

Zhou, X., Liao, W.J., Liao, J.M., Liao, P., and Lu, H. (2015b). Ribosomal proteins: functions beyond the ribosome. J. Mol.Cell Biol. *7*, 92–104.

iScience, Volume *23*

Supplemental Information

Dynamic Malignant Wave of Ribosome-Insulted Gut Niche via the Wnt-CTGF/CCN2 Circuit

Ki Hyung Kim, Seung Joon Lee, Juil Kim, and Yuseok Moon

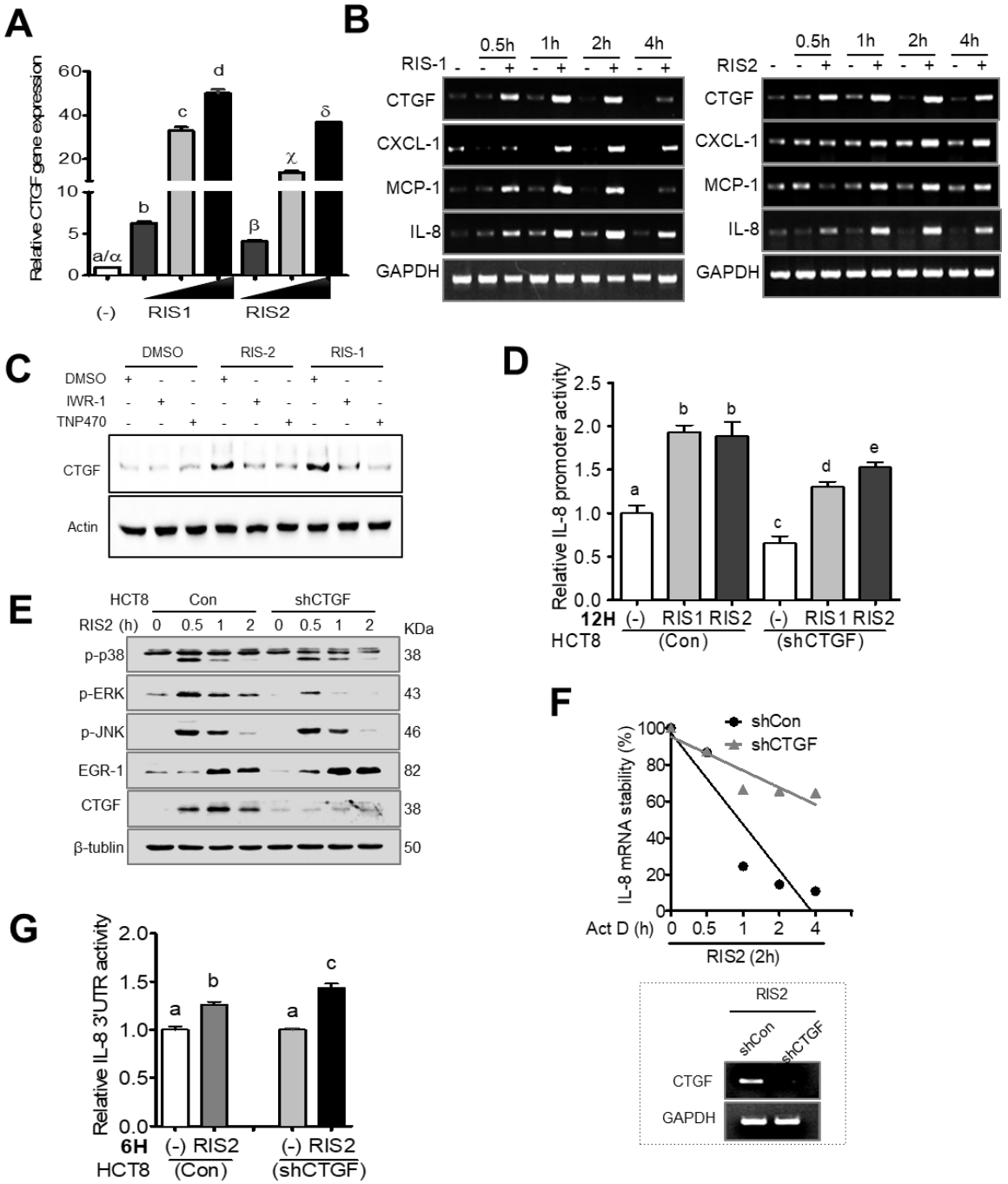

Figure S1. Roles of CTGF/CCN2 in regulation of proinflammatory chemokine. (A) Quantitative real-time RT-PCR (qRT-PCR) for CTGF in HCT8 cells in response to serially-increasing doses of RIS-1 and RIS-2. Dosages of RIS-1 and RIS-2 were 10, 50, and 100 ng/mL and 50, 100, and 500 ng/mL, respectively. Results are shown as mean values ± SEM. (B) Semi-quantitative RT-PCR for proinflammatory cytokines in HCT8 cells subjected to time-dependent exposure to 50 ng/mL RIS-1 (left) or 500 ng/mL of RIS-2 (right). (C) HCT8 cells were treated with either IWR-1 (30 μM) or TNP470 (10 μM) for 6 h prior to 2 h of exposure to RIS-1 (50 ng/mL) or RIS-2 (500 ng/mL), then examined by western blotting. (D) IL-8 promoter activity of control or CTGF-deficient HCT8 cells treated with either RIS-1 (50 ng/mL) or RIS-2 (500 ng/mL) for 12 h. Results are shown as mean values ± SEM. (E) Control and CTGF knockdown HCT8 cells were treated with 500 ng/mL RIS-2 for 0.5, 1, or 2 h, then examined by western blotting. (F) Actinomycin D (Act D)-mediated IL-8 mRNA stability after RIS-2 treatment for 2 h and corresponding linear regression analysis. Slopes of CTGF-deficient (shCTGF, gray triangles) and control groups (shCon, black circles) were −46.12 ± 14.82 and −17.50 ± 6.43, respectively. (G) IL-8 3'UTR activity of HCT8 in response to RIS-2 (500 ng/mL) treatment for 6 h. Results are shown as mean values ± SEM. Different letters over each box represent statistically significant differences among groups based on one-way ANOVA ($p < 0.05$).

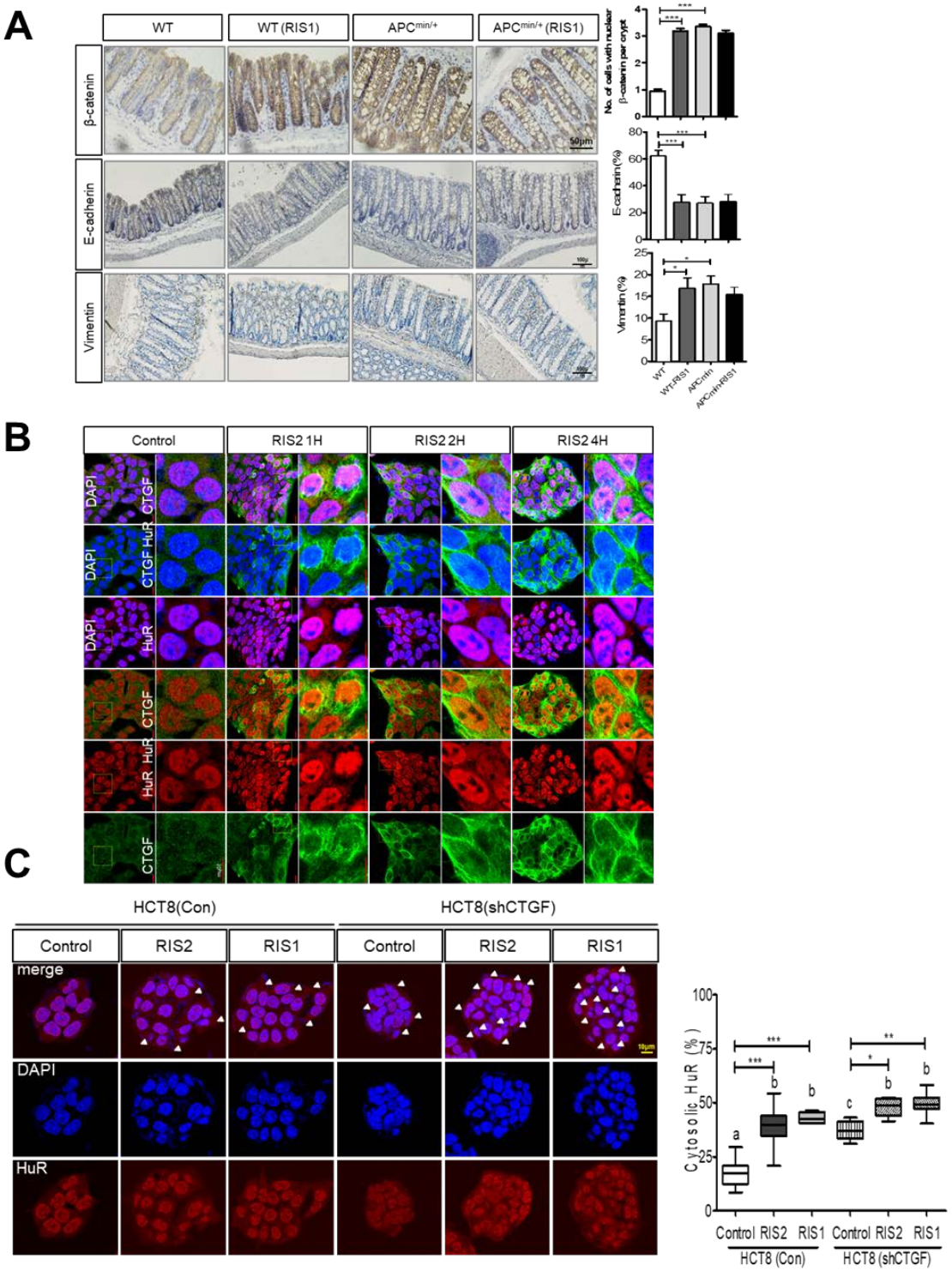

Figure S2. Effects of ribosomal insults on EMT and related signaling. (A) Immunohistochemistry of β -catenin and EMT makers in colons of wild type and APC$^{min/+}$ mice exposed to vehicle control or RIS-1 (25 mg/kg) by oral gavage for 72 h. Results are shown as mean values ± SEM. Asterisks represent statistically significant values (*p<0.05, **p<0.01, ***p<0.001). (B) Immunostaining of HCT-8 cells with CTGF (FITC), HuR (Texas red) and DAPI after treatment with 500 ng/mL of RIS-2 for 1 h to 4 h. Co-localization patterns of HuR with CTGF were categorized based on cytosolic and nuclear compartments. (C) Cytosolic translocation of HuR in response to treatment with 500 ng/mL RIS-2 or 50 ng/ml RIS-1 for 1 h in control and CTGF-deficient HCT8 cells. HCT8 cells were immunostained with HuR then staining quantified and statistically evaluated by ANOVA. White arrowheads indicate cells with cytosolic HuR. Results are shown as box-and-whisker plots (min to max). The different letters over each box represent statistically significant differences among groups based on one-way ANOVA ($p < 0.05$).

Fig. S2

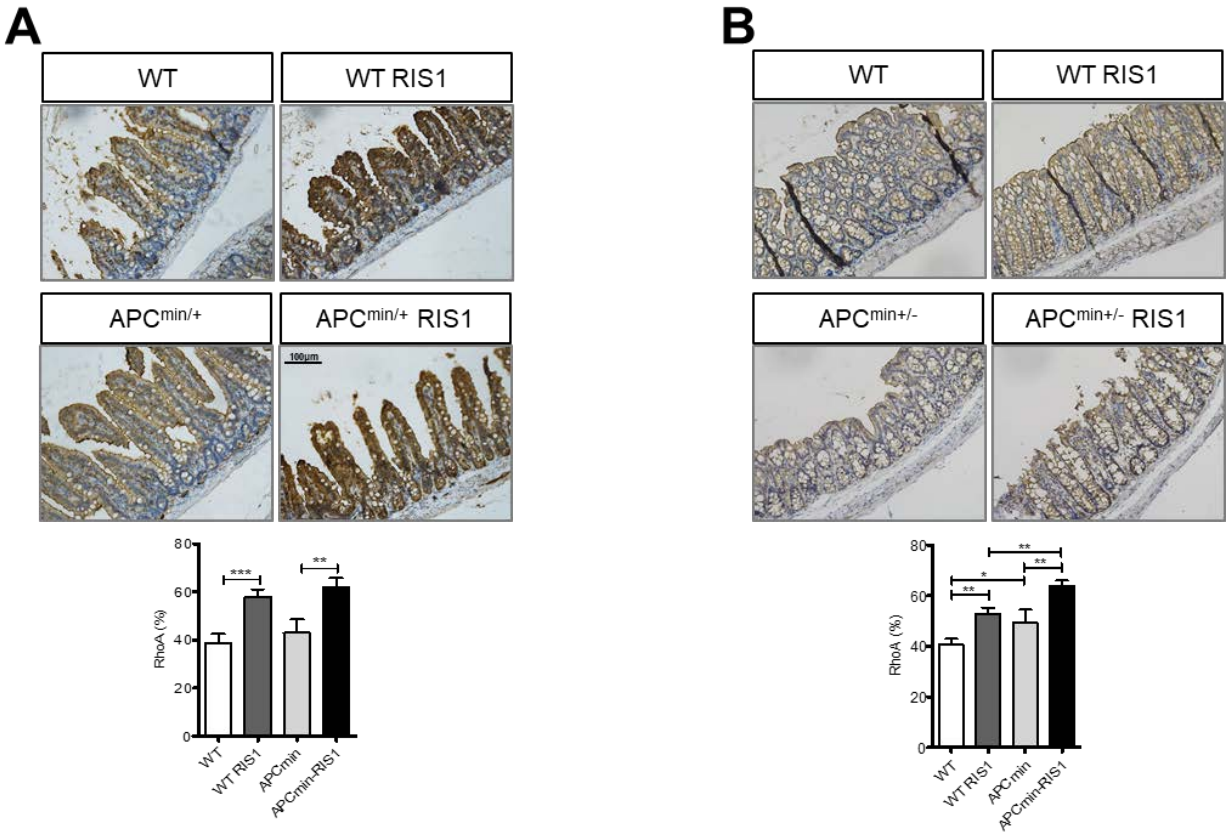

Figure S3. Wnt/PCP-linked signaling in ribosome-insulted CRC. Immunohistochemistry of RhoA in small (A) and large (B) intestines of WT and APC$^{min/+}$ mice exposed to vehicle control or RIS-1 for 72 h (25 mg/kg, oral gavage), which were statistically analyzed using HistoQuest software. Results are shown as mean values ± SEM. Asterisks represent statistically significant values (*p < 0.05, **p < 0.01, ***p < 0.001).

Fig. S3

TRANSPARENT METHODS

Animal experiments and ethics. Animal care and experiments were conducted in accordance with the guidelines of the Pusan National University Institutional Animal Care and Use Committee (PNUIACUC; Approval Number PNU-2017-1555) and the Guide for the Care and Use of Laboratory Animals from the National Institutes of Health. $APC^{min/+}$ mice were kindly provided by Dr. Kangyeol Choi of Yonsei University. RIS-1 (anisomycin, 25 mg/kg body weight) was administered to 8-week-old $APC^{min-/+}$ and C57BL6 control mice. After 72 h, intestines were assessed by immunohistochemistry and staining with trichrome, hematoxylin, and eosin. For xenograft assays, $2.1x10^6$ HCT8 spheroid cells were dissociated into single cells, resuspended in 100 µL of PBS, and subcutaneously injected into a lateral flank region of SCID nude mice (KOATECH, Korea). The incidence and size of xenografted tumors were determined every week until sacrifice.

Genomic analysis using public datasets. Results involving patients with colon adenocarcinomas are based on data (TCGA-COAD, n = 440) from the Cancer Genome Atlas (TCGA) Research Network: http://cancergenome.nih.gov/. Other clinical sources of genomic data from colorectal cancer tissue samples are from CRC patients in *Sieber*'s dataset (GEO ID: gse14333, n=290).

2.3. Cell culture and reagents. HCT8, HCT116, DLD1, LOVO, SW480, HEK293, and HT29 cells were purchased from the American Type Culture Collection (ATCC, Manassas, VA, USA). Cancer cell lines were maintained in RPMI 1640 medium while HEK293 cells were maintained in DMEM. Both media types were supplemented with

10% heat-inactivated fetal bovine serum (FBS), 50 units/mL penicillin, and 50 mg/mL streptomycin (Welgene, Daegu, South Korea) and cell lines maintained in a 5% CO_2, humidified atmosphere at 37°C. Cell counts were performed using a hemocytometer with a trypan blue (Sigma-Aldrich, St. Louis, MO, USA) dye exclusion assay to identify viable cells. All other reagents, including RIS-inducing agents RIS-1 (anisomycin) and RIS-2 (deoxynivlaenol), were purchased from Sigma-Aldrich.

Spheroid culture and flow cytometry. A total of $2.5x10^5$ HCT8 cells per well were seeded in ultra-low attachment 6-well plates (Costar #3471) with DMEM/F12 medium supplemented with B27, 20 ng/mL epidermal growth factor (EGF) (BD science), 20 ng/mL basic fibroblast growth factor, 50 units/mL penicillin, and 50 μg/mL streptomycin in a 5% CO_2 humidified atmosphere at 37°C. Cells were pre-exposed to 500 ng/mL of RIS-2 or 50 ng/mL RIS-1 in combination with other inhibitors for 24 h, washed with DMEM/F12 twice, then cultured for 6 days. Spheroid cells were dissociated into single cells with trypsin, washed with PBS, incubated with FITC-conjugated CD44 (BD Science) and APC-conjugated CD133 (Mylteic) antibodies for 15 min at 4°C. CD44 and CD133 expression was then assessed using a Becton Dickinson FACS Canto II (BD Bioscience, San Jose, CA, USA)

CRC cell line-based organoid culture. Cells were pre-exposed to 500 ng/mL RIS-2 or 50 ng/mL RIS-1 in combination with other inhibitors for 24 h, washed with DMEM/F12 twice, then cultured for 6 days in the spheroid culture media defined above. A suspension of 200–400 spheroids with approximately 100 μm diameters was seeded into individual wells of a 24-well tissue culture plate with equal volumes of matrigel (BD #354324). Spheroids were then cultured in IntestiCult™ Organoid Growth

Medium (STEM CELLS # 06011 and # 06012) containing 10 μM Y-27632 for 12 d. The morphology of cultured CRC organoids was evaluated along with immunostaining for E-cadherin and Mucin-2.

Plasmid construction. CMV-driven short hairpin RNAs (shRNAs) were constructed by inserting an shRNA into pSilencer 4.1-CMV-neo vector (Ambion, Austin, TX, USA). Vectors containing negative control shRNAs or shRNAs targeting either CTGF or HuR are labelled Con, shCTGF, or shHuR, respectively. The negative control shRNA template sequence lacks significant homology to the mouse, human, and rat genome databases. The pSilencer 4.1-CMV neo vector containing the negative control shRNA template was provided by Ambion. Sequences for shRNAs targeting CTGF and HuR were 5′-CAC CAG CAT GAA GAC ATA C-3′ and 5′- GTG CAA AGG GTT TGG CTT T-3′, respectively.

Immunoblotting. Protein expression levels were assessed by immunoblotting. Briefly, cultured cells were harvested in SDS-lysis buffer and lysed using a sonicator. Proteins were quantified using the WelProt^{TM} protein Assay reagent (Welgene, Daegu, South Korea), after which cell lysates were separated via electrophoresis (BioRad, Hercules, CA, USA) and transferred to polyvinylidene fluoride membranes (Amersham Bioscience, Piscataway, NJ, USA). Blots were blocked with 5% skim milk in 0.1% TBST for 2 h then probed with primary antibody overnight at 4°C. After washing three times with TBST, blots were incubated with horseradish-conjugated secondary antibodies for 2 h then washed four times with TBST for 10 min per wash. ECL substrate (ELPIS Biotech, Taejon, South Korea)-based chemiluminescent signals were detected and quantified using a FUSION Solo S (Vilber Lourmat, France). Antibody

dilutions used for immunoblotting were as follows: CTGF/CCN2 (Santa Cruz Biotechnology, Santa Cruz, CA, USA 1:500); p-ERK, p-JNK, p-p38, activated β-catenin (ABC), and p-GSK3β (Cell signaling, 1:1,000); hnRNP, EGR-1, β-catenin, HuR, hnRNP, actin, and β-tubulin (Santa Cruz Biotechnology, Santa Cruz, CA, USA 1:1,000); anti-rabbit secondary (Enzo Life Science, Plymouth Meeting, PA, USA); anti-mouse secondary (Enzo Life Science, Plymouth Meeting, PA, USA); anti-goat secondary (Santa Cruz Biotechnology, Santa Cruz, CA, USA).

Reverse Transcription (RT) PCR and Real-time PCR. RNA was extracted using RiboEX (GeneAll Biotechnology, Seoul, South Korea) according to the manufacturer's instructions. RNA (100 ng) from each sample was then transcribed into cDNA using Moloney murine leukemia virus reverse transcriptase (Genetbio, Nonsan, South Korea), after which specific genes were amplified using N-Taq DNA polymerase (Enzynomics, Seoul, South Korea) in a MyCycler thermal cycler (BioRad). For real-time PCR, the fluorescent reporter dye FAM was conjugated to the 5′ ends of probes used to detect amplified cDNA in an iCycler thermal cycler (BioRad).

Immunocytochemistry. Cells **(**$1x10^5$) were seeded in a glass-bottomed 35 mm cell culture plate and the treated cells were fixed with 4% paraformaldehyde for 10 min, washed with PBS, permeabilized with 0.3% BSA and 0.2% Triton X-100 in PBS for 10 min, then blocked with 3% bovine serum albumin (BSA) in PBS for 2 h. Next, cells were stained with anti-goat CTGF/CCN2 (1:200), anti-mouse HuR (1:200), DAPI (1:1000), FITC-conjugated anti-goat IgG, Texas Red-conjugated anti-mouse IgG, or Alexa594-conjugated anti rabbit IgG (1:200). Stained cells were analyzed by confocal microscopy (FluoView FV1000, Olympus). For immunostaining of spheroid cells,

cultured spheroid cells were fixed with 1% triton X-100 and 4% paraformaldehyde for 12 h then subjected to additional fixation with 4% paraformaldehyde. Fixed spheroid cells were subsequently washed with PBS and immunostained with CD44-FTIC (BD science). Stained spheroid cells were analyzed by confocal microscopy (FluoView FV1000, Olympus) using Z-stacks ranging from depths of 60–80 μm. Stacked images were projected onto the Y-axis and 3-dimensional hemisphere images made using 3D rendering to examine the presence of CD44-FITC-positive cancer stem cells within the heterogeneous collection of spheroid tumor cells.

Immunohistochemistry and histological staining. To analyze spatial expression patterns of markers in intestinal tissues, immunohistochemistry, hematoxylin, eosin, or trichrome staining were performed according to standard protocols. The following antibodies were used for immunohistochemistry: CTGF/CCN2 (1:100, Santa Cruz); HuR (1:200, Santa Cruz); E-cadherin (1:200, Santa Cruz); Vimentin (1:200, Santa Cruz); α-SMA (1:200, Santa Cruz); β-catenin (1:200, Santa Cruz); RhoA (1:100, Santa Cruz). The amount of 3,3′-diaminobenzidine (DAB)-positive cells and hematoxylin-positive cells were quantified using HistoQuest software (TissueGnostics) and statistically analyzed with an unpaired two-tailed t-test. Trichrome staining was performed to examine compositional changes of connective tissues according to the manufacturer's instructions (Abcam, ab150686). Briefly, sections were deparaffinized then hydrated in an ethanol series (100% to 50%). Next, slides were immersed in preheated Bouin's fluid for 60 min then rinsed in tap water. Nuclei were then stained with working Weigert's Iron Hematoxylin solution for 5 min. After another rinse with running tap water, slides were covered in Biebrich Scarlet/Acid Fuchsin solution to stain acidophilic tissue components, such as cytoplasm and muscle fibers, until collagen

was no longer red. Phosphomolybdic/phosphotungstic acid solution was then applied to each section, after which collagen in each sample was stained with aniline blue then samples transferred to 1% acetic acid for 5 min for destaining. Stained sections were subsequently dehydrated very quickly with two changes of 95% ethyl alcohol, followed by two changes of absolute alcohol, after which samples were cleared in xylene and mounted in synthetic mountant (Thermo Scientific, 6769007). This process stained connective tissues, including collagen, stained blue, nuclei dark red/purple, and cytoplasm or muscle fibers red/pink. Quantification of the *de novo* connective tissue was conducted using Prism 5 (GraphPad Software, San Diego, CA, USA).